

Hydrogen gas post-conditioning attenuates early neuronal pyroptosis in a rat model of subarachnoid hemorrhage through the mitoK_{ATP} signaling pathway

CHUAN-SUO ZHANG¹, QIAN HAN², ZHAO-WEI SONG¹,
HONG-YAN JIA¹, TIAN-PENG SHAO¹ and YAN-PENG CHEN¹

Departments of ¹Radioactive Intervention and ²Anesthesiology,
Cangzhou Central Hospital, Cangzhou, Hebei 061000, P.R. China

Received September 12, 2020; Accepted May 12, 2021

DOI: 10.3892/etm.2021.10268

Abstract. Neuronal pyroptosis serves an important role in the progress of neurologic dysfunction following subarachnoid hemorrhage (SAH), which is predominantly caused by a ruptured aneurysm. Hydrogen gas has been previously reported to be an effective anti-inflammatory agent against ischemia-associated diseases by regulating mitochondrial function. The objective of the present study was to investigate the potential neuroprotective effects of hydrogen gas post-conditioning against neuronal pyroptosis after SAH, with specific focus on the mitochondrial ATP-sensitive K⁺ (mitoK_{ATP}) channels. Following SAH induction by endovascular perforation, rats were treated with inhalation of 2.9% hydrogen gas for 2 h post-perforation. Neurologic deficits, brain water content, reactive oxygen species (ROS) levels, neuronal pyroptosis, phosphorylation of ERK1/2, p38 MAPK and pyroptosis-associated proteins IL-1 β and IL-18 were evaluated 24 h after perforation by a modified Garcia method, ratio of wet/dry weight, 2',7'-dichlorofluorescein diacetate, immunofluorescence and western blot assays, respectively. An inhibitor of the mitoK_{ATP} channel, 5-hydroxydecanoate sodium (5-HD), was used to assess the potential role of the mitoK_{ATP}-ERK1/2-p38 MAPK signal pathway. Hydrogen gas post-conditioning significantly alleviated brain edema and improved neurologic function, reduced ROS production and neuronal pyroptosis, suppressed the expression of IL-1 β and IL-18 whilst upregulating ERK1/2 phosphorylation, but downregulated p38 MAPK activation 24 h post-SAH. These aforementioned effects neuroprotective were partially

reversed by 5-HD treatment. Therefore, these observations suggest that post-conditioning with hydrogen gas ameliorated SAH-induced neuronal pyroptosis at least in part through the mitoK_{ATP}/ERK1/2/p38 MAPK signaling pathway.

Introduction

Aneurysmal subarachnoid hemorrhage (SAH) is a common cause of stroke that usually results in undesirable outcomes and is associated with a high mortality rate around the world of 50% (1,2). Neuronal pyroptosis has been suggested to be a key factor in the process of early brain injury (3). Upregulation of the melanoma 2 (AIM2) inflammasome, which is activated by double-stranded DNA from mitochondria and nuclei, leads to neuronal pyroptosis in a mouse model of SAH (4). In addition, calcium overload has also been suggested to be involved in neuronal pyroptosis after SAH (5). Previous studies have reported that early brain injury, which is characterized by an inflammatory response prior to cerebral vasospasm, leads to disability or even mortality post-SAH (6,7). Therefore, investigations into the potential effective anti-pyroptotic strategies have been gathering attention as therapy for patients with SAH.

A number of studies have reported that inhalation of hydrogen gas significantly attenuates oxidative stress, exhibits anti-pyroptosis and anti-inflammatory activities and reduces cerebral ischemia/reperfusion injury in rodent models (8-10). Zhan *et al* (2) demonstrated that hydrogen gas exerts protective effects against early brain injury post-SAH, which was mediated by inhibiting oxidative stress. It has also been reported that hydrogen gas attenuates inflammatory responses in the heart and liver after organ transplantation (11,12). Mitochondrial regulation, including those of mitochondrial ATP-sensitive K⁺ (mitoK_{ATP}) channels, serves a role in the neuroprotective effects of hydrogen gas (13,14). In addition, hydrogen gas has been suggested to activate both proliferating and pro-apoptotic signaling cascades, including the ERK1/2 or p38 MAPK (15-17). However, the exact mechanism by which hydrogen gas protects against SAH-induced neurologic dysfunction remains poorly understood.

Correspondence to: Dr Chuan-Suo Zhang, Department of Radioactive Intervention, Cangzhou Central Hospital, 16 Xinhua Street, Cangzhou, Hebei 061000, P.R. China
E-mail: 2146878560@qq.com

Key words: hydrogen gas, post-conditioning, pyroptosis, subarachnoid hemorrhage, mitochondrial ATP-sensitive potassium channel

Opening of mitoK_{ATP} channels, in addition to the activation of ERK1/2 and p38 MAPK have all been reported to underlie the neuroprotective effects of hydrogen gas as aforementioned. Therefore, in the present study, the potential therapeutic effects of hydrogen gas post-conditioning on a SAH-induced rat model of neuronal pyroptosis and the mitoK_{ATP}/ERK1/2/p38 MAPK signal pathway induced by intravascular perforation was investigated.

Materials and methods

Animals. In total, 137 male Sprague-Dawley rats (Liaoning Changsheng Biotechnology Co., Ltd.) weighing 324±13 g (age, 9-10 weeks) were utilized in the present study. Under controlled conditions, the rats were exposed to a regular 12 h light/dark cycle (lights on at 7:00 a.m. and lights off at 7:00 p.m.). The room temperature was maintained at 25±1°C and the humidity was kept at 50±10%. Rats were allowed free access to standard diet and water.

According to a random number table, rats were divided into the following five groups: i) Sham (n=24); ii) SAH (n=30); iii) SAH plus treatment with 2.9% hydrogen post-conditioning for 2 h (SAH + H₂; n=25); iv) SAH treatment with an intraperitoneal injection (i.p.) pre-injection of 5-hydroxydecanoate sodium (5-HD; 40 mg/kg; cat. no. ab141672; Abcam) followed by 2.9% hydrogen post-conditioning for 2 h (SAH + H₂ + 5-HD; n=31); and v) SAH treatment with pre-injection of saline containing an equivalent concentration of DMSO and 2.9% hydrogen post-conditioning for 2 h (SAH + H₂ + saline; n=27).

SAH was initiated by intravascular perforation on the bifurcation of the anterior cerebral artery and the middle cerebral artery. Rats in the H₂ groups inhaled 2.9% hydrogen mixed with 20% oxygen and balanced nitrogen (flow rate, 1 l/min) immediately after SAH for 2 h. Rats in the 5-HD groups were administered 5-HD (40 mg/kg i.p.) at 30 min before SAH. Rats in the saline groups were administered with saline containing an equivalent concentration of DMSO i.p. The animal protocols included in the present study were ratified by the Institutional Animal Care and Use Committee at The Cangzhou Central Hospital (Cangzhou, China).

SAH model and hydrogen administration. Intravascular perforation was performed to simulate SAH in a rat model (18). Compared with two injections of arterial blood solvates into the cisterna magna, the rat endovascular perforation model was considered to be the more representative model of human SAH (19). Briefly, under sevoflurane anesthesia [induction (7-8%) and maintenance (3-4%)], rats were intubated and then ventilated at a tidal volume of 4 ml/100 g (fraction of inspired oxygen, 40%) using ventilators (Shanghai Alcott Biological Technology Inc.). The rectal temperature was maintained at 36.0±0.5°C using a heating pad. The left external carotid artery was then ligated, following which a sharpened 5-0 suture line was placed from the stump of the external carotid artery. The vessel wall located on the bifurcation of the anterior and middle cerebral arteries was perforated. The sham-operated rats also underwent the same procedure but the arteries were not perforated. The rats in the H₂ groups inhaled 2.9% hydrogen mixed with 20% oxygen and balanced nitrogen (Gilmore Liquid Air Company) at a flow rate of

1 l/min immediately after SAH for 2 h under anesthesia. The hydrogen concentration was discontinuously monitored using a handheld hydrogen detector (H₂scan Corporation) every 10 min. After post-conditioning of hydrogen gas, the rats were freely allowed access to water and food in separate animal facilities. The health and behavior including respiratory function of rats were monitored every hour within 24 h. If any of the rats were unable to eat food or drink water, or breathed slowly and weakly, euthanasia was performed via cervical dislocation under sevoflurane anesthesia within 24 h after SAH. According to a previous study (18), the severity of SAH was assessed by a SAH grading scale. Following decapitating under anesthesia (8% sevoflurane) and the removal of brains 24 h post-SAH, the bases of the brains were pictured. Six segments of the basal cistern base were allocated a grade from 0 to 3 (0, no SAH; 1, minimal subarachnoid blood; 2, mediocre blood with visible arteries; 3, blood clots covering all arteries). The SAH grade was calculated using the sum of the six scores from the six segments.

Neurobehavioral test. A modified method of Garcia *et al* (20) was used 24 h post-SAH to evaluate neurologic behavior in the rats (n=6 per group) (20). The modified Garcia method ranged from 0 to 18 points, including spontaneous activity (0-3 points), symmetry in forelimb movement (0-3 points), forepaw outstretching (0-3 points), climbing (0-3 points), body proprioception (0-3 points) and response to vibrissae touch (0-3 points). The conductors (ZWS and HYJ), who were blinded to the group information of the rats, assessed the aforementioned neurologic parameters of the rats.

Brain water content. The rats were decapitated under anesthesia (8% sevoflurane) 24 h post-SAH before the brain tissues were immediately isolated from the skull and dissected into right and left hemispheres, cerebellum and brain stem (n=6 per group). After weighing (wet weight), all tissues were dehydrated for 72 h in a 105°C oven and weighed again (dry weight). The following formula was used to assess brain water content: [(Wet weight-dry weight)/wet weight] x100%.

Reactive oxygen species (ROS) production. Rats were perfused through the left ventricle-ascending aorta with cold saline under anesthesia (8% sevoflurane) 24 h post-SAH (n=6 per group). Compared with right hemisphere, left hemisphere is associated with more significant changes in oxidative stress and inflammatory parameters (21). The cortical tissue from the left hemisphere was lysed in RIPA buffer (cat. no. P0013C; Beyotime Institute of Biotechnology) and quantified using the BCA protein assay. The mixture containing cortical tissues (0.1 ml containing 1 mg), ROS assay medium (2.9 ml; D-PBS, cat. no. C0221D; Beyotime Institute of Biotechnology) and 2',7'-dichlorofluorescein diacetate (5 nmol/μl; cat. no. S0033S; Beyotime Institute of Biotechnology) was incubated at 37°C for 15 min. The fluorescence intensity was used to assess ROS production through a microplate reader (485 nm excitation wavelength; 525 nm emission wavelength; Bio-Rad Laboratories, Inc.).

Immunofluorescence. Rats were perfused via the left ventricle-ascending aorta with cold saline under anesthesia

(8% sevoflurane) 24 h post-SAH and then re-infused with 10% neutral-buffered formalin (n=6 per group). After fixation with 10% neutral-buffered formalin for 48 h at room temperature, the brain tissues were embedded in paraffin. Brain tissues were then sectioned (4 μ m thick), dewaxed by xylene and gradient-hydrated by ethanol at room temperature. After boiling with 3% sodium citrate at 100°C for 20 min, the slices were blocked with QuickBlock™ Blocking Buffer for Immunol Staining (cat. no. P0260; Beyotime Institute of Biotechnology) for 1 h at room temperature and subsequently incubated with primary monoclonal rabbit antibodies against cleaved caspase-1 (1:500; cat. no. 4199; Cell Signaling Technology, Inc.) and polyclonal mouse anti-rat-neuronal nuclei (NeuN; 1:500; cat. no. ab104224; Abcam) at 4°C overnight. After rinsing with PBS three times, the sections were incubated with the secondary antibodies (FITC-conjugated goat anti-rabbit IgG; 1:500; cat. no. A0562; and Cy3-conjugated goat anti-mouse IgG, 1:500; cat. no. A0521; Beyotime Institute of Biotechnology) for 1 h at room temperature. Finally, the cell nuclei were stained with DAPI (5 μ g/ml per section; Beyotime Institute of Biotechnology) for 5 min at room temperature. A fluorescence microscope (MF43; Guangzhou Micro-shot Technology Co., Ltd.) was used to observe six fields of view at magnifications of x200 and x1,000 in three sections randomly selected from each group. In each field, the average density of the fluorescence signals were measured using the Image-pro plus 6.0 software (Media Cybernetics, Inc.). Cells labeled with cleaved caspase-1 and NeuN were defined as pyroptotic before being counted.

Western blotting. Following ice-saline perfusion via the left ventricle-ascending aorta under anesthesia (8% sevoflurane), the cortical tissue from the left hemisphere was lysed in RIPA buffer (cat. no. P0013C; Beyotime Institute of Biotechnology) and assembled to extract total protein (n=6 per group) 24 h post-SAH. Each sample contained 40 μ g protein and was separated by 10% SDS-PAGE. The separated protein was then transferred onto PVDF membranes (Beyotime Institute of Biotechnology). After blocking with buffer (cat. no. P0252, QuickBlock™ Western Blocking Buffer; Beyotime Institute of Biotechnology) at 25°C for 10 min, polyclonal rabbit anti-rat IL-1 β antibody (1:1,000; cat. no. K107559P; Beijing Solarbio Science & Technology Co., Ltd.), polyclonal rabbit anti-rat IL-18 antibody (1:1,000, cat. no. K002143P; Beijing Solarbio Science & Technology Co., Ltd.), monoclonal rabbit anti-rat phosphorylated (p)-ERK1/2 antibody (1:1,000, cat. no. AF1891; Beyotime Institute of Biotechnology), monoclonal rabbit anti-rat ERK1/2 antibody (1:1,000, cat. no. AF1051; Beyotime Institute of Biotechnology) antibodies, polyclonal rabbit anti-rat p-p38 antibody (1:1,000, cat. no. AF5887; Beyotime Institute of Biotechnology), and polyclonal rabbit anti-rat p38 antibody (1:1,000, cat. no. AF7668; Beyotime Institute of Biotechnology) were applied overnight at 4°C. HRP-labeled goat anti-rabbit secondary antibodies (1:1,000, cat. no. A0208; Beyotime Institute of Biotechnology) were used to incubate the membranes at room temperature for 1 h. After rinsing with Western Wash Buffer (cat. no. P0023C; Beyotime Institute of Biotechnology), the PVDF membranes were incubated

with BeyoECL Moon reagent (cat. no. P0018FM; Beyotime Institute of Biotechnology) for 5 min. A western blotting detection system (Gel Doc XRS, Bio-Rad Laboratories, Inc.) was used to visualize the density of protein bands on the PVDF membranes. GAPDH (1:1,000; cat. no. K106389P; Beijing Solarbio Science & Technology Co., Ltd.) was used as an internal reference and membranes were incubated with this overnight at 4°C (22). All western blotting bands were semi-quantified using Image Lab software 6.0.1 (Bio-Rad Laboratories, Inc.).

Statistical analysis. Fisher's exact test with Bonferroni's correction was used to assess the difference in mortality between groups (sham vs. SAH, SAH vs. SAH + H₂, SAH + H₂ vs. SAH + H₂ + 5-HD, SAH + H₂ + 5-HD vs. SAH + H₂ + saline and SAH + H₂ vs. SAH + H₂ + saline). The data of neurobehavioral tests are presented as the median + interquartile range and further analyzed by Kruskal-Wallis followed by Dunn's post hoc test. The remaining data are expressed as the mean \pm SD. Statistical differences between the various groups were evaluated by one-way analysis of variance and Tukey's test. The statistical analysis was assessed by the SPSS 11.0 software (SPSS, Inc.) and the level of statistically significant difference was considered at P<0.05.

Results

Mortality. Prior to scheduled euthanasia, 17 rats died due to cerebral hernia. A total of 5 rats were euthanized due to reaching humane endpoints such as slow and weak breath, and the remaining 12 rats had died prior to post-operative monitoring. The mortality rate within 24 h post-SAH was 0% (0 of 24 rats) in the sham group, 20% (6 of 30 rats) in the SAH group, 4% (1 of 25 rats) in the SAH + H₂ group, 22.6% (7 of 31 rats) in the SAH + H₂ + 5-HD group and 11.1% (3 of 27 rats) in the SAH + H₂ + saline group, and there was no significant difference between sham and SAH, SAH and SAH + H₂, SAH + H₂ and SAH + H₂ + 5-HD, SAH + H₂ 5-HD and SAH + H₂ + saline, SAH + H₂ and SAH + H₂ + saline groups (Fig. 1A). A total of 16 rats died within 6 h after SAH and 1 rat died at 18 h after SAH. Compared with rats in the sham group, the average SAH grades were significantly increased in rats with SAH exposure in the other four groups (Fig. 1B). There was no significant statistical difference in the average SAH grades among the remaining four groups based on the SAH grade (18) (Fig. 1B). This finding indicated a similar degree of bleeding among the groups.

Neurobehavioral test. Compared with that in rats in the sham group, neurologic function of the rats in the SAH group was significantly impaired 24 h after the SAH-operation (P<0.05; Fig. 2). Hydrogen gas post-conditioning after SAH induction significantly improved the neurobehavioral score in rats compared with that in rats treated with SAH alone 24 h post-SAH (P<0.05; Fig. 2). By contrast, whilst 5-HD partially but significantly reversed the changes mediated by hydrogen gas in the neurobehavioral score in rats (P<0.05; Fig. 2). There was no statistically significant difference in the neurological scores of rats between the SAH + H₂ and SAH + H₂ + saline groups (Fig. 2).

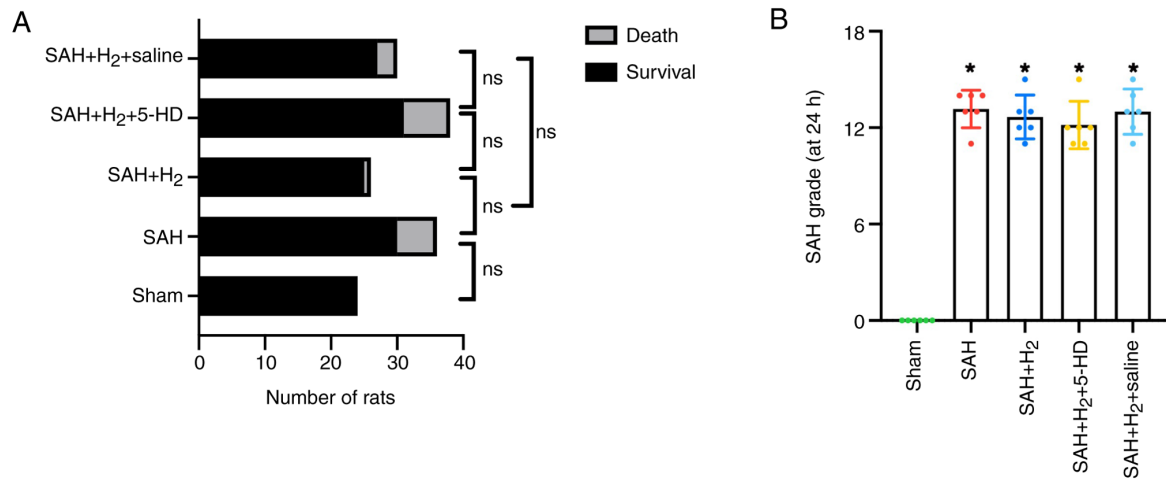


Figure 1. (A) Comparison of the number of rats that survived and those that died in each treatment group. Fisher's exact test followed by Bonferroni's correction was used. (B) Quantification of the severity of SAH. A summary of SAH scores for the six groups is presented (n=6). *P<0.05 vs. Sham. SAH, subarachnoid hemorrhage; 5-HD, 5-hydroxydecanoate sodium; ns, not significant.

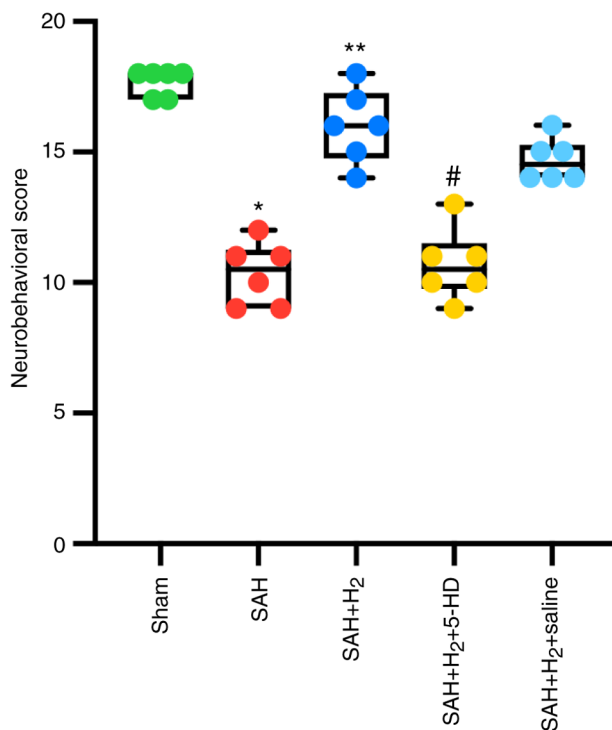


Figure 2. Changes in neurological dysfunction as assessed by neurobehavioral tests at 24 h after SAH induction and various indicated treatments. Data are presented as the median + interquartile range (n=6 per group). *P<0.05 vs. Sham; **P<0.05 vs. SAH; #P<0.05 vs. SAH + H₂. SAH, subarachnoid hemorrhage; 5-HD, 5-hydroxydecanoate sodium.

Brain water content. SAH exposure significantly increased the water content in the bilateral hemispheres, including the right hemisphere (P<0.001), left hemisphere (P<0.001; Fig. 3), cerebellum (P<0.001; Fig. 3) and the brain stem (P<0.001; Fig. 3) of rats compared with that in the rats in the sham group 24 h post-perforation. Hydrogen gas post-conditioning significantly improved brain edema in the right hemisphere (P<0.001; Fig. 3), left hemisphere (P<0.001; Fig. 3), cerebellum (P<0.05; Fig. 3) and the brain stem (P<0.05; Fig. 3) compared with that in the SAH group. It was shown that these attenuations

induced by hydrogen gas post-conditioning were partially but significantly reversed by 5-HD administration (left hemisphere, P<0.05; right hemisphere, P<0.05; cerebellum, P<0.05; brain stem, P<0.05; Fig. 3). Additionally, as a control for 5-HD, saline administration after SAH + H₂ treatment failed to show a significant reversion compared with that after SAH + H₂ treatment alone (Fig. 3).

ROS production. The level of ROS production in the cortex was significantly upregulated 24 h post-perforation in the SAH group compared with that in the Sham group (P<0.05; Fig. 4). ROS production in cortex, however, was significantly lower in rats exposed to hydrogen gas post-conditioning after SAH induction compared with that after SAH alone (P<0.05; Fig. 4). 5-HD significantly elevated ROS production in the cortex compared with that in the SAH + H₂ group (P<0.05; Fig. 4). However, there was no significant difference in cortex ROS production between the SAH + H₂ and SAH + H₂ + saline groups (Fig. 4).

Measurement of pyroptosis. Neuronal pyroptosis in the ipsilateral cortex was assessed by immunofluorescence after labeling with cleaved caspase-1- and NeuN-specific antibodies. The levels of cleaved caspase-1 and NeuN co-staining were significantly elevated 24 h post-perforation in the SAH group compared with those in the Sham group (P<0.05; Fig. 5B). Compared with that in the SAH group, hydrogen gas post-conditioning significantly attenuated neuronal pyroptosis, as indicated by the reduced number of dual cleaved caspase-1 and NeuN-positive cells in the SAH + H₂ group (P<0.05; Fig. 5B). Inhibition of mitoK_{ATP} opening using 5-HD significantly increased neuronal pyroptosis in the SAH + H₂ + 5-HD group compared with that in the SAH + H₂ group (P<0.05; Fig. 5B). In addition, there was no significant difference in neuronal pyroptosis between the SAH + H₂ and SAH + H₂ + saline groups (Fig. 5).

Pyroptosis-associated proteins IL-1 β and IL-18, was investigated further by western blotting. The expression levels of IL-1 β (P<0.05; Fig. 6B) and IL-18 (P<0.05; Fig. 6C) in protein samples collected from the ipsilateral cortex was significantly

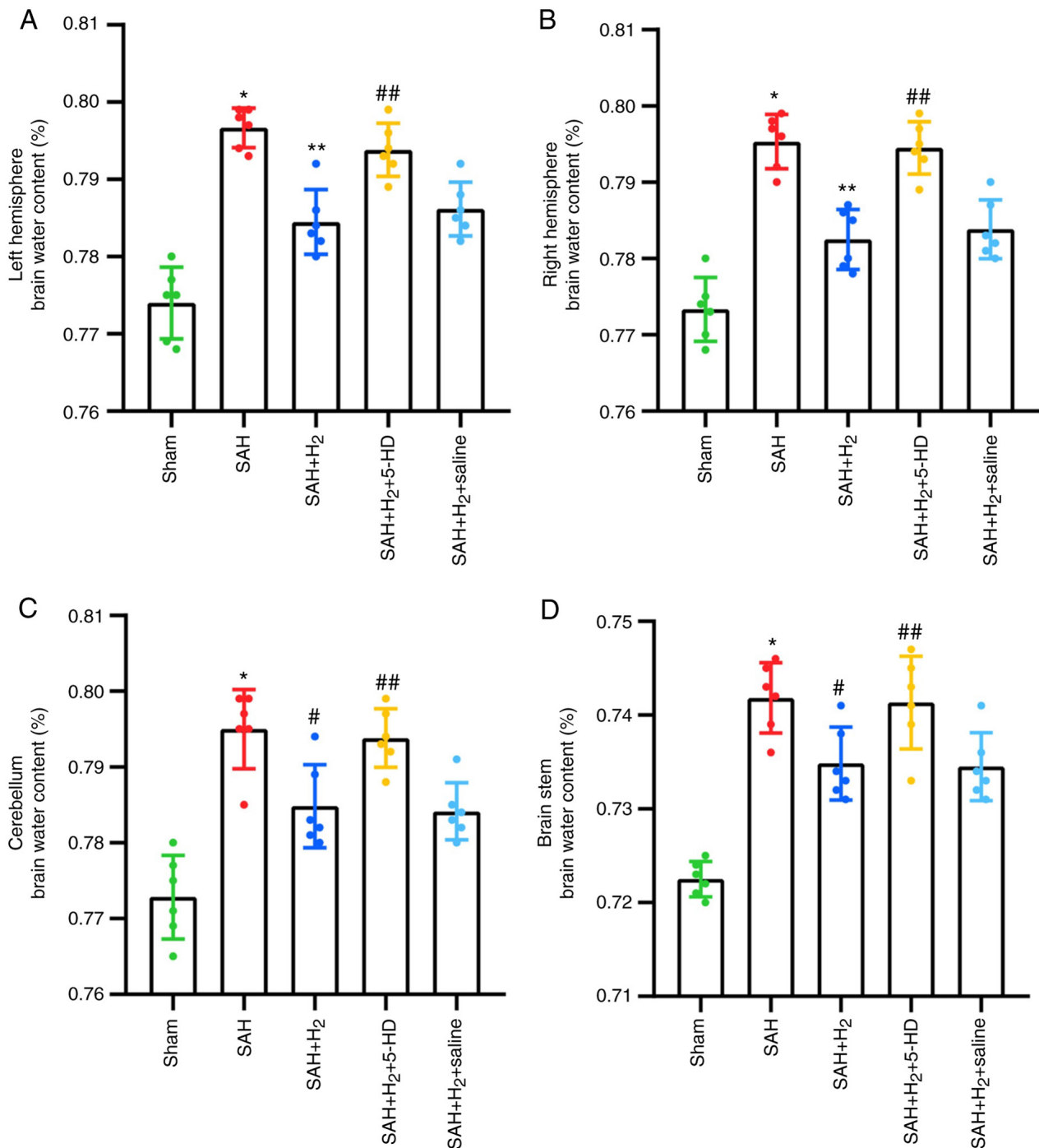


Figure 3. Analysis of brain edema after SAH induction. Changes in water content in (A) the left hemisphere, (B) right hemisphere, (C) cerebellum and (D) brain stem following the indicated treatment at 24 h after SAH induction. Data are presented as the mean \pm SD (n=6 per group). *P<0.001 vs. Sham; **P<0.001 vs. SAH in the left and right hemisphere; #P<0.05 vs. SAH in the cerebellum and brain stem; ##P<0.05 vs. SAH + H₂. SAH, subarachnoid hemorrhage; 5-HD, 5-hydroxydecanoate sodium.

upregulated in rats exposed to SAH compared with those in samples from the Sham group. Hydrogen gas post-conditioning significantly attenuated the increases in IL-1 β (P<0.05; Fig. 6B) and IL-18 (P<0.05; Fig. 6C) compared with those in the SAH alone group. Consistent with the results from immunofluorescence, 5-HD significantly reversed the alleviation of hydrogen gas post-conditioning in the SAH + H₂ + 5-HD group (IL-1 β , P<0.05; IL-18, P<0.05; Fig. 6B and C). No significant difference was reported in the expression of IL-1 β and IL-18 between the SAH + H₂ and SAH + H₂ + saline groups (Fig. 6).

Phosphorylated ERK1/2 and p38 MAPK levels. Increased levels of p-ERK1/2 (P<0.05; Fig. 7B) and p-p38 MAPK (P<0.05; Fig. 7C) were observed in the SAH group compared with those in the Sham group. Hydrogen gas post-conditioning potentiated the levels of ERK1/2 phosphorylation significantly further (P<0.05; Fig. 7B), whilst significantly reducing the phosphorylation of p38 MAPK (P<0.05; Fig. 7C) compared with those in the SAH only group. A significant reduction in p-ERK1/2 (P<0.05; Fig. 7B) and increase in p-p38 MAPK (P<0.05; Fig. 7C) were detected in rats exposed to 5-HD

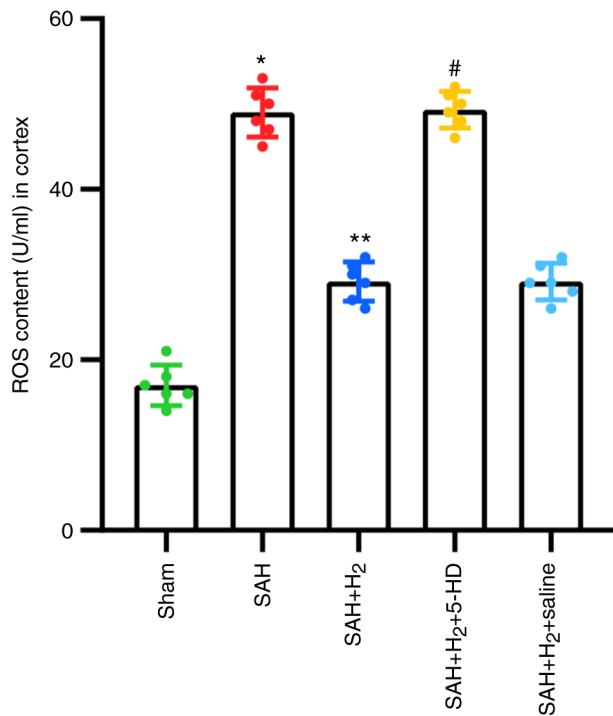


Figure 4. Changes in ROS levels following the indicated treatments 24 h after subarachnoid SAH. Data are presented as the mean \pm SD (n=6 per group). *P<0.05 vs. Sham; **P<0.05 vs. SAH; #P<0.05 vs. SAH + H₂. SAH, subarachnoid hemorrhage; 5-HD, 5-hydroxydecanoate sodium; ROS, reactive oxygen species.

treatment compared with those in rats in the SAH + H₂ group. Additionally, there was no significant difference in the levels of p-ERK1/2 and p-p38 MAPK between the SAH + H₂ and SAH + H₂ + saline groups (Fig. 7).

Discussion

The present study investigated the potential therapeutic effects of hydrogen gas post-conditioning against neurological dysfunction, brain edema, ROS production and neuronal pyroptosis in a rat model of SAH. It was found that the neuroprotective effects mediated by hydrogen gas against SAH-induced injury could be at least in part downstream of the mitoK_{ATP} channels (Fig. 8).

Cerebral vasospasm after SAH could lead to ischemia/reperfusion, which causes mitochondrial dysfunction (23,24). Mitochondrial dysfunction after SAH leads to the release of damage-associated molecular patterns (DAMPs), including ROS, mitochondrial DNA and calcium ions (25-27). DAMPs can induce the activation of cytoplasmic inflammasome complexes, including caspase-1, adaptor protein apoptosis-associated speck-like protein containing a CARD and NOD-like receptor (28). Consequently, activated caspase-1 is activated to drive the proteolytic cleavage and maturation of precursor cytokines, including pro-IL-1 β and pro-IL-18 (29). Moreover, ROS is likely to serve a major role in activation of caspase-1, which induces pyroptosis and leads to cellular edema (30). A number of previous studies have demonstrated that SAH-induced brain injury can be alleviated by modulating ROS and caspase-dependent

neuronal death (31-33). In agreement with a previous study, brain edema and cortical neuronal pyroptosis was observed in a SAH model, where the pathologic changes may be attributed to deficits in neurologic function (34). In addition, it was also shown that brain edema occurred on bilateral hemisphere regardless of the perforation side (2).

It was previously reported that hydrogen gas administration attenuated not only ischemic infarction in the brain, but also reduced hemorrhagic transformation induced by hyperglycemia in a model of middle cerebral artery occlusion (MCAO) (35,36). In addition, hydrogen gas administration exerted significant anti-inflammatory activity against ischemia/reperfusion injury in various organ transplantations, including the heart and liver (37,38). Hydrogen gas can be explosive at concentrations >5%, but it is neither explosive nor dangerous at low concentrations (39). In the present study, 2.9% hydrogen gas post-conditioning for 2 h after SAH was used according to a previous study (2). In addition, 2.9% hydrogen gas inhalation for 2 h ameliorated neurologic dysfunction, alleviated brain edema and attenuated neuronal pyroptosis, whereby suggesting that hydrogen gas post-conditioning can confer therapeutic effects in a SAH rat model.

Neuroprotective effects of exogenous hydrogen gas has been previously reported to be associated with mitochondrial regulation (40). Watanabe *et al* (41) reported that the opening/activation of mitoK_{ATP} channels are involved in delaying neuroprotection in a Mongolian gerbil model of MCAO. As a specific inhibitor, 5-HD has been applied as an approach to study the involvement of mitoK_{ATP} channels (42). A previous study showed that the mitoK_{ATP} channels in heart and liver mitochondria are the targets for 5-HD, by the inhibition of K⁺ flux (43). The present study therefore assessed the effects of mitoK_{ATP} opening on the neuroprotective effects of hydrogen gas using 5-HD. 5-HD was found to partially reverse the therapeutic effects of neurologic dysfunction, attenuation of brain edema and amelioration of neuronal pyroptosis induced by hydrogen gas post-conditioning after SAH exposure. These results suggest that the neuroprotective effects of hydrogen gas post-conditioning may be associated with mitoK_{ATP} channels opening.

The downstream mechanisms underlying mitoK_{ATP} channels in the central nervous system remained unclear. A previous study reported that the opening of mitoK_{ATP} channels is associated with the increased levels of phosphorylated ERK1/2 after cerebral ischemia/reperfusion injury (44). It has also been suggested that the downregulation of p38 MAPK phosphorylation contributes to the improvements in cerebral ischemia/reperfusion in mice (45,46). Chen *et al* (47) demonstrated that caspase-1-related pyroptosis is inhibited by downregulation of p38 phosphorylation MAPK and upregulation of ERK1/2 in mice. The MC4 receptor agonist RO27-3225 inhibited NLRP1-dependent neuronal pyroptosis via the ASK1/JNK/p38 MAPK pathway in a mouse model of intracerebral haemorrhage (47). The changes in cellular potassium and mitochondrial membrane potential induced by the opening of mitoK_{ATP} channels is likely to contribute to changes in p38 MAPK and ERK1/2 phosphorylation (48,49). Data from the present study showed that hydrogen gas significantly elevated levels of ERK1/2 phosphorylation but

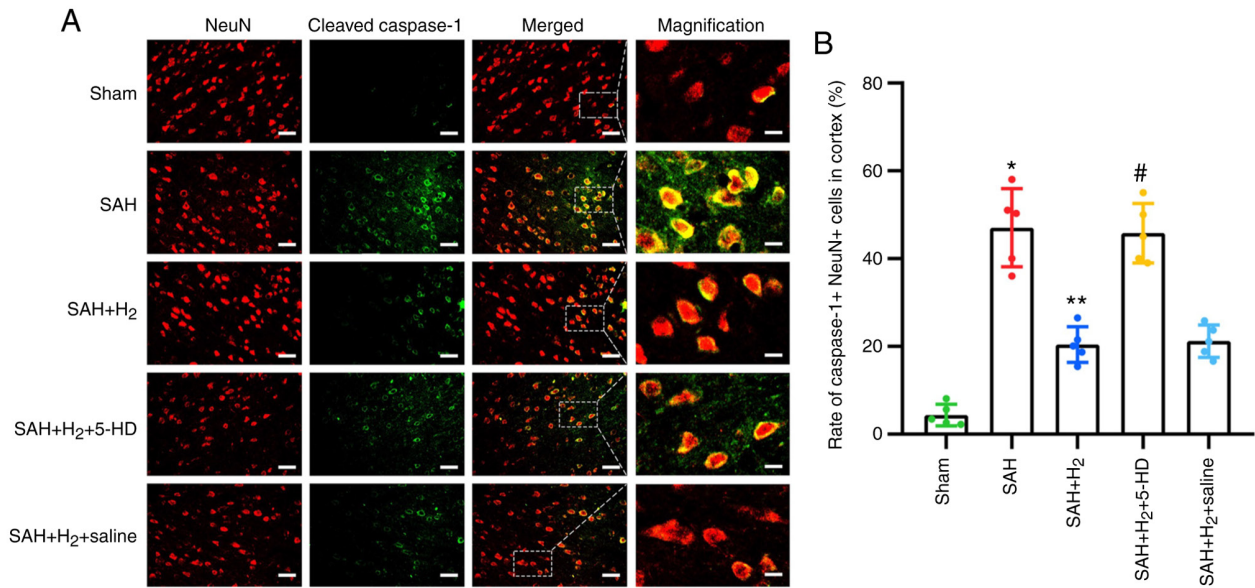


Figure 5. Changes in neuronal pyroptosis in the cortical tissue caused following the indicated treatment. (A) Representative photomicrographs of cleaved caspase-1, NeuN and DAPI staining showing pyroptotic cells in the cortical tissue by the indicated treatment at 24 h after SAH. Corresponding magnified merged staining images are shown on the far right panel. Cleaved caspase-1, green; NeuN, red; DAPI, blue. Scale bars, 50 or 12.5 μ m. (B) Percentages of pyroptotic cells in the cortical tissue caused by the indicated treatment. Data are presented as the mean \pm SD (n=6 per group). *P<0.05 vs. Sham; **P<0.05 vs. SAH; #P<0.05 vs. SAH + H₂. SAH, subarachnoid hemorrhage; 5-HD, 5-hydroxydecanoate sodium; NeuN, neuronal nuclei.

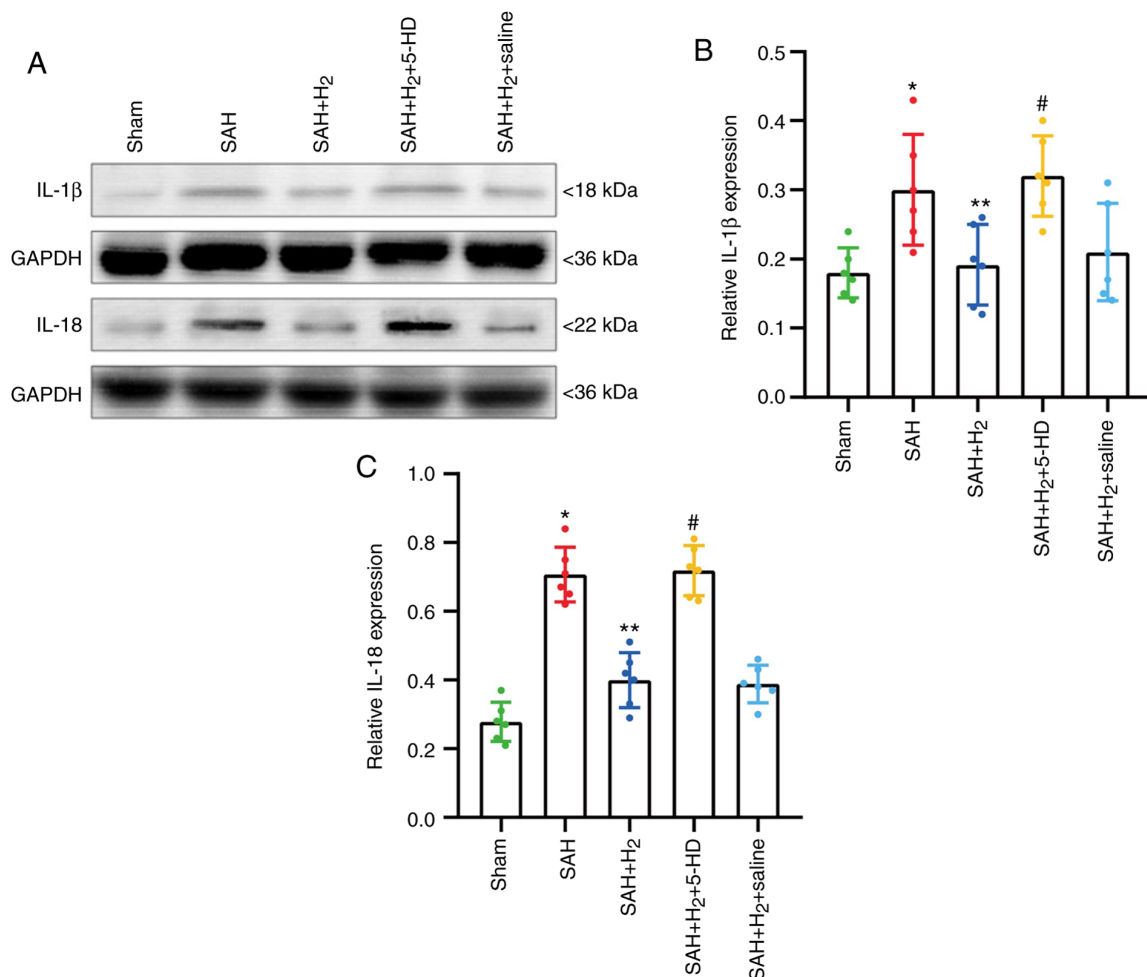


Figure 6. Changes in the expression of proteins associated with pyroptosis following the indicated treatment. (A) Representative western blotting images of IL-1 β and IL-18 in the cortical tissue. Quantified expression of (B) IL-1 β and (C) IL-18, normalized to that of GAPDH. Data are presented as the mean \pm SD (n=6 per group). *P<0.05 vs. Sham; **P<0.05 vs. SAH; #P<0.05 vs. SAH + H₂. SAH, H₂, 5-HD and saline are as described previously; SAH, subarachnoid hemorrhage; 5-HD, 5-hydroxydecanoate sodium.

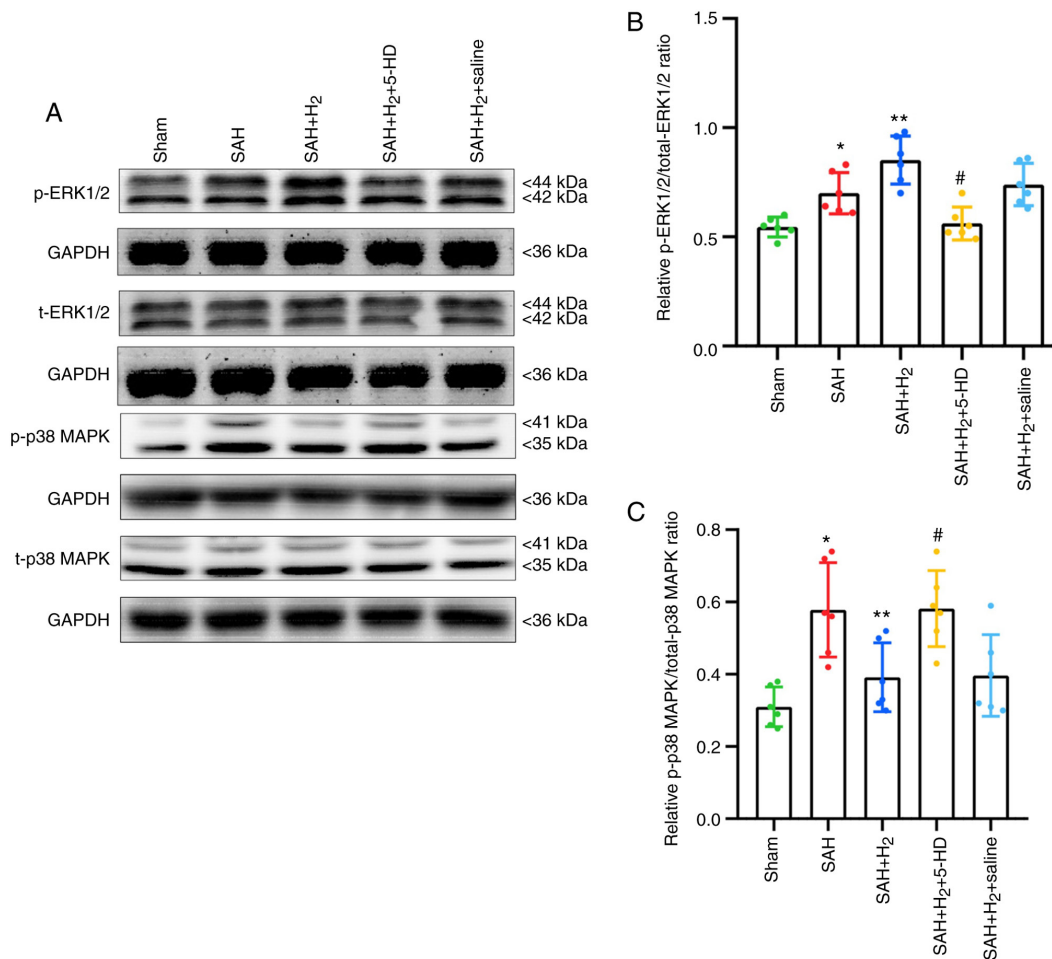


Figure 7. Changes in the phosphorylation levels of ERK1/2 and p38 MAPK following the indicated treatment. (A) Representative western blotting images of phosphorylated ERK1/2, total ERK1/2, phosphorylated p38 and total p38 MAPK in the cortical tissue. Expression of (B) phosphorylated ERK1/2 and total ERK1/2, (C) phosphorylated p38 and total p38 MAPK was quantified following normalization to that of GAPDH. Data are presented as the mean \pm SD (n=6 per group). *P<0.05 vs. Sham; **P<0.05 vs. SAH; #P<0.05 vs. SAH + H₂. SAH, subarachnoid hemorrhage; 5-HD, 5-hydroxydecanoate sodium; NeuN, neuronal nuclei; p-, phosphorylated; t-, total.

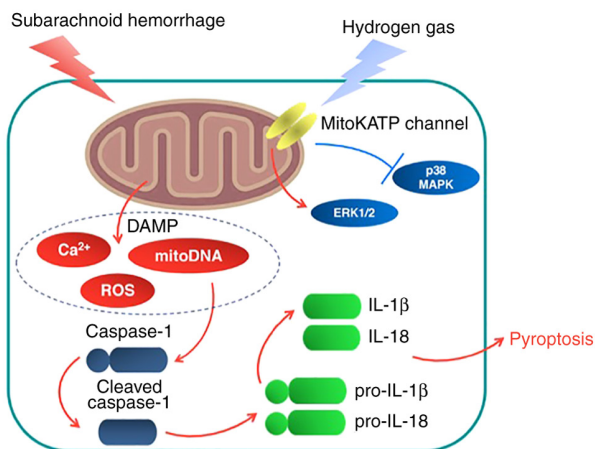


Figure 8. Proposed model from the present study. A proposed schematic summarizing the observations following hydrogen gas post-conditioning and subsequent neuroprotection against SAH. SAH increased neuronal pyroptosis, which hydrogen gas post-conditioning not only significantly attenuated, but also improved neurological dysfunction further downstream. This may be associated with increased ERK1/2 phosphorylation and phosphor-decreased p38 MAPK activation by opening mitoK_{ATP}. 5-HD, an inhibitor of mitoK_{ATP}, could partially reverse these neuroprotective effects. DAMP, damage associated molecular patterns; mitoK_{ATP}, mitochondrial ATP-sensitive K⁺ channels.

attenuated levels of p38 MAPK phosphorylation. However, 5-HD partially reversed this upregulation of p-ERK1/2 and downregulation of p-p38 MAPK induced by exogenous hydrogen gas. Such a dichotomy of these two kinases, including p38 MAPK and ERK1/2, was suggested to be involved in neuronal death induced by cardiopulmonary resuscitation injury (50). In addition, hydrogen gas opened mitoK_{ATP} channels through direct interaction with Cys6 and Cys26, which regulate the cellular energy charge to activate the downstream MAPK pathways (51). Therefore, it could be hypothesized from these aforementioned observations that activation of the mitoK_{ATP}/ERK1/2/p38 MAPK pathway might be involved as a potential target of exogenous hydrogen gas.

One limitation of the present study was that the neuroprotective effects of hydrogen gas 24 h post-SAH were only observed in this animal model. Long term changes in neurologic function, brain edema and neuronal pyroptosis, such as 72 h and 1 week after SAH, should be investigated. In addition, only a single application of hydrogen gas was achieved for 2 h after SAH exposure. The potential therapeutic effects of repeated applications of hydrogen gas post-SAH should also be explored.

In conclusion, the present study found that hydrogen gas post-conditioning exhibited significant neuroprotective effects against in early-stage SAH, possibly through an anti-pyroptosis effect downstream of the mitoK_{ATP}/ERK1/2/p38 MAPK signal pathway. Therefore, exogenous hydrogen gas has the potential to improve early injury during the management of SAH.

Acknowledgements

Not applicable.

Funding

The present study was supported by the Medical Science Plan of Hebei Province of China (grant no. 20211745).

Availability of data and materials

The datasets used and/or analyzed during the present study are available from the corresponding author on reasonable request.

Authors' contributions

CSZ was responsible for the design of the study. QH and CSZ were responsible for statistical analysis. CSZ, QH, ZWS, HYJ, TPS and YPC were responsible for the experiments and data collection. CSZ and QH confirm the authenticity of all the raw data. All authors have read and approved the final manuscript.

Ethics approval and consent to participate

The animal protocols included in the present study were ratified by the Institutional Animal Care and Use Committee at The Cangzhou Central Hospital (Cangzhou, China).

Patient consent for publication

Not applicable.

Competing interests

The authors declare that they have no competing interests.

References

- Yang C, Li T, Xue H, Wang L, Deng L, Xie Y, Bai X, Xin D, Yuan H, Qiu J, *et al*: Inhibition of necroptosis rescues SAH-induced synaptic impairments in hippocampus via CREB-BDNF pathway. *Front Neurosci* 12: 990, 2019.
- Zhan Y, Chen C, Suzuki H, Hu Q, Zhi X and Zhang JH: Hydrogen gas ameliorates oxidative stress in early brain injury after subarachnoid hemorrhage in rats. *Crit Care Med* 40: 1291-1296, 2012.
- Xu P, Hong Y, Xie Y, Yuan K, Li J, Sun R, Zhang X, Shi X, Li R, Wu J, *et al*: TREM-1 exacerbates neuroinflammatory injury via NLRP3 inflammasome-mediated pyroptosis in experimental subarachnoid hemorrhage. *Transl Stroke Res*: Aug 30, 2020 (Epub ahead of print).
- Yuan B, Zhou XM, You ZQ, Xu WD, Fan JM, Chen SJ, Han YL, Wu Q and Zhang X: Inhibition of AIM2 inflammasome activation alleviates GSDMD-induced pyroptosis in early brain injury after subarachnoid haemorrhage. *Cell Death Dis* 11: 76, 2020.
- Zhou K, Enkhjargal B, Xie Z, Sun C, Wu L, Malaguit J, Chen S, Tang J, Zhang J and Zhang JH: Dihydrolipoic acid inhibits lysosomal rupture and NLRP3 through lysosome-associated membrane protein-1/calcium/calmodulin-dependent protein kinase II/TAK1 pathways after subarachnoid hemorrhage in rat. *Stroke* 49: 175-183, 2018.
- Ruan W, Hu J, Zhou H, Li Y, Xu C, Luo Y, Chen T, Xu B, Yan F and Chen G: Intranasal wnt-3a alleviates neuronal apoptosis in early brain injury post subarachnoid hemorrhage via the regulation of wnt target PPAN mediated by the moonlighting role of aldolase C. *Neurochem Int* 134: 104656, 2020.
- Shao A, Wu H, Hong Y, Tu S, Sun X, Wu Q, Zhao Q, Zhang J and Sheng J: Hydrogen-rich saline attenuated subarachnoid hemorrhage-induced early brain injury in rats by suppressing inflammatory response: Possible involvement of NF- κ B pathway and NLRP3 inflammasome. *Mol Neurobiol* 53: 3462-3476, 2016.
- Ohsawa I, Ishikawa M, Takahashi K, Watanabe M, Nishimaki K, Yamagata K, Katsura K, Katayama Y, Asoh S and Ohta S: Hydrogen acts as a therapeutic antioxidant by selectively reducing cytotoxic oxygen radicals. *Nat Med* 13: 688-694, 2007.
- Xie K, Zhang Y, Wang Y, Meng X, Wang Y, Yu Y and Chen H: Hydrogen attenuates sepsis-associated encephalopathy by NRF2 mediated NLRP3 pathway inactivation. *Inflamm Res* 69: 697-710, 2020.
- Ono H, Nishijima Y, Ohta S, Sakamoto M, Kinone K, Horikosi T, Tamaki M, Takeshita H, Futatuki T, Ohishi W, *et al*: Hydrogen gas inhalation treatment in acute cerebral infarction: A randomized controlled clinical study on safety and neuroprotection. *J Stroke Cerebrovasc Dis* 26: 2587-2594, 2017.
- Zhang Y, Tan S, Xu J and Wang T: Hydrogen therapy in cardiovascular and metabolic diseases: From bench to bedside. *Cell Physiol Biochem* 47: 1-10, 2018.
- Uto K, Sakamoto S, Que W, Shimata K, Hashimoto S, Sakisaka M, Narita Y, Yoshii D, Zhong L, Komohara Y, *et al*: Hydrogen-rich solution attenuates cold ischemia-reperfusion injury in rat liver transplantation. *BMC Gastroenterol* 19: 25, 2019.
- Walewska A, Szewczyk A and Koprowski P: Gas signaling molecules and mitochondrial potassium channels. *Int J Mol Sci* 19: 3227, 2018.
- Oh GS, Pae HO, Lee BS, Kim BN, Kim JM, Kim HR, Jeon SB, Jeon WK, Chae HJ and Chung HT: Hydrogen sulfide inhibits nitric oxide production and nuclear factor- κ B via heme oxygenase-1 expression in RAW264.7 macrophages stimulated with lipopolysaccharide. *Free Radic Biol Med* 41: 106-119, 2006.
- Carreras MC and Poderoso JJ: Mitochondrial nitric oxide in the signaling of cell integrated responses. *Am J Physiol Cell Physiol* 292: C1569-C1580, 2007.
- Zhai Y, Zhou X, Dai Q, Fan Y and Huang X: Hydrogen-rich saline ameliorates lung injury associated with cecal ligation and puncture-induced sepsis in rats. *Exp Mol Pathol* 98: 268-276, 2015.
- King AL and Lefer DJ: Cytoprotective actions of hydrogen sulfide in ischaemia-reperfusion injury. *Exp Physiol* 96: 840-846, 2011.
- Sugawara T, Ayer R, Jadhav V, Chen W, Tsubokawa T and Zhang JH: Simvastatin attenuation of cerebral vasospasm after subarachnoid hemorrhage in rats via increased phosphorylation of Akt and endothelial nitric oxide synthase. *J Neurosci Res* 86: 3635-3643, 2008.
- Sehba FA: The rat endovascular perforation model of subarachnoid hemorrhage. *Acta Neurochir Suppl* 120: 321-324, 2015.
- Garcia JH, Wagner S, Liu KF and Hu XJ: Neurological deficit and extent of neuronal necrosis attributable to middle cerebral artery occlusion in rats. Statistical validation. *Stroke* 26: 627-635, 1995.
- Liu W, Li R, Yin J, Guo S, Chen Y, Fan H, Li G, Li Z, Li X, Zhang X, *et al*: Mesenchymal stem cells alleviate the early brain injury of subarachnoid hemorrhage partly by suppression of Notch1-dependent neuroinflammation: Involvement of botch. *J Neuroinflammation* 16: 8, 2019.
- Zhang DX, Zhang LM, Zhao XC and Sun W: Neuroprotective effects of erythropoietin against sevoflurane-induced neuronal apoptosis in primary rat cortical neurons involving the EPOR-Erk1/2-Nrf2/Bach1 signal pathway. *Biomed Pharmacotherapy* 87: 332-341, 2017.
- Zhang XX, He FF, Yan GL, Li HN, Li D, Ma YL, Wang F, Xu N and Cao F: Neuroprotective effect of cerebralcaere granule after cerebral ischemia/reperfusion injury. *Neural Regen Res* 11: 623-629, 2016.

24. Huang S, Li H and Ge J: A cardioprotective insight of the cystathionine γ -lyase/hydrogen sulfide pathway. *Int J Cardiol Heart Vasc* 7: 51-57, 2015.
25. Wellman GC: Ion channels and calcium signaling in cerebral arteries following subarachnoid hemorrhage. *Neurol Res* 28: 690-702, 2006.
26. Chaudhry SR, Frede S, Seifert G, Kinfe TM, Niemelä M, Lamprecht A and Muhammad S: Temporal profile of serum mitochondrial DNA (mtDNA) in patients with aneurysmal subarachnoid hemorrhage (aSAH). *Mitochondrion* 47: 218-226, 2019.
27. Zhou K, Shi L, Wang Z, Zhou J, Manaenko A, Reis C, Chen S and Zhang J: RIP1-RIP3-DRP1 pathway regulates NLRP3 inflammasome activation following subarachnoid hemorrhage. *Exp Neurol* 295: 116-124, 2017.
28. Van Opendenbosch N, Gurung P, Vande Walle L, Fossoul A, Kanneganti TD and Lamkanfi M: Activation of the NLRP1b inflammasome independently of ASC-mediated caspase-1 autoproteolysis and speck formation. *Nat Commun* 5: 3209, 2014.
29. Samir P, Kesavardhana S, Patmore DM, Gingras S, Malireddi RKS, Karki R, Guy CS, Briard B, Place DE, Bhattacharya A, *et al*: DDX3X acts as a live-or-die checkpoint in stressed cells by regulating NLRP3 inflammasome. *Nature* 573: 590-594, 2019.
30. Hoque R, Sohail M, Malik A, Sarwar S, Luo Y, Shah A, Barrat F, Flavell R, Gorelick F, Husain S and Mehal W: TLR9 and the NLRP3 inflammasome link acinar cell death with inflammation in acute pancreatitis. *Gastroenterology* 141: 358-369, 2011.
31. Zhang ZY, Jiang M, Fang J, Yang MF, Zhang S, Yin YX, Li DW, Mao LL, Fu XY, Hou YJ, *et al*: Enhanced therapeutic potential of nano-curcumin against subarachnoid hemorrhage-induced blood-brain barrier disruption through inhibition of inflammatory response and oxidative stress. *Mol Neurobiol* 54: 1-14, 2017.
32. Zhang Z, Liu J, Fan C, Mao L, Xie R, Wang S, Yang M, Yuan H, Yang X, Sun J, *et al*: The GluN1/GluN2B NMDA receptor and metabotropic glutamate receptor 1 negative allosteric modulator has enhanced neuroprotection in a rat subarachnoid hemorrhage model. *Exp Neurol* 301: 13-25, 2018.
33. Wang W, Han P, Xie R, Yang M, Zhang C, Mi Q, Sun B and Zhang Z: TAT-mGluR1 attenuation of neuronal apoptosis through prevention of MGlur1 α truncation after experimental subarachnoid hemorrhage. *ACS Chem Neurosci* 10: 746-756, 2019.
34. Chen J, Zhang C, Yan T, Yang L, Wang Y, Shi Z, Li M and Chen Q: Atorvastatin ameliorates early brain injury after subarachnoid hemorrhage via inhibition of pyroptosis and neuroinflammation. *J Cell Physiol*: Mar 31, 2021 (Epub ahead of print).
35. Chen L, Chao Y, Cheng P, Li N, Zheng H and Yang Y: UPLC-QTOF/MS-based metabolomics reveals the protective mechanism of hydrogen on mice with ischemic stroke. *Neurochem Res* 44: 1950-1963, 2019.
36. Chen CH, Manaenko A, Zhan Y, Liu WW, Ostrowki RP, Tang J and Zhang JH: Hydrogen gas reduced acute hyperglycemia-enhanced hemorrhagic transformation in a focal ischemia rat model. *Neuroscience* 169: 402-414, 2010.
37. Buchholz BM, Kaczorowski DJ, Sugimoto R, Yang R, Wang Y, Billiar TR, McCurry KR, Bauer AJ and Nakao A: Hydrogen inhalation ameliorates oxidative stress in transplantation induced intestinal graft injury. *Am J Transplant* 8: 2015-2024, 2008.
38. Yao L, Chen H, Wu Q and Xie K: Hydrogen-rich saline alleviates inflammation and apoptosis in myocardial I/R injury via PINK-mediated autophagy. *Int J Mol Med* 44: 1048-1062, 2019.
39. Ohno K, Ito M, Ichihara M and Ito M: Molecular hydrogen as an emerging therapeutic medical gas for neurodegenerative and other diseases. *Oxid Med Cell Longev* 2012: 353152, 2012.
40. Noda M, Liu J and Long J: Neuroprotective and preventative effects of molecular hydrogen. *Curr Pharm Des* 27: 585-591, 2021.
41. Watanabe M, Katsura K, Ohsawa I, Mizukoshi G, Takahashi K, Asoh S, Ohta S and Katayama Y: Involvement of mitoKATP channel in protective mechanisms of cerebral ischemic tolerance. *Brain Res* 1238: 199-207, 2008.
42. Garlid KD, Paucek P, Yarov-Yarovoy V, Murray HN, Darbenzio RB, D'Alonzo AJ, Lodge NJ, Smith MA and Grover GJ: Cardioprotective effect of diazoxide and its interaction with mitochondrial ATP-sensitive K⁺ channels. Possible mechanism of cardioprotection. *Circ Res* 81: 1072-1082, 1997.
43. Jaburek M, Yarov-Yarovoy V, Paucek P and Garlid KD: State-dependent inhibition of the mitochondrial KATP channel by glyburide and 5-hydroxydecanoate. *J Biol Chem* 273: 13578-13582, 1998.
44. Naitoh K, Ichikawa Y, Miura T, Nakamura Y, Miki T, Ikeda Y, Kobayashi H, Nishihara M, Ohori K and Shimamoto K: MitoKATP channel activation suppresses gap junction permeability in the ischemic myocardium by an ERK-dependent mechanism. *Cardiovasc Res* 70: 374-383, 2006.
45. Bu X, Huang P, Qi Z, Zhang N, Han S, Fang L and Li J: Cell type-specific activation of p38 MAPK in the brain regions of hypoxic preconditioned mice. *Neurochem Int* 51: 459-466, 2007.
46. Li J, Lang MJ, Mao XB, Tian L and Feng YB: Antiapoptosis and mitochondrial effect of pioglitazone preconditioning in the ischemic/reperfused heart of rat. *Cardiovasc Drugs Ther* 22: 283-291, 2008.
47. Chen S, Zuo Y, Huang L, Sherchan P, Zhang J, Yu Z, Peng J, Zhang J, Zhao L, Doycheva D, *et al*: The MC₄ receptor agonist RO27-3225 inhibits NLRP1-dependent neuronal pyroptosis via the ASK1/JNK/p38 MAPK pathway in a mouse model of intracerebral haemorrhage. *Br J Pharmacol* 176: 1341-1356, 2019.
48. Subramaniam S, Strelau J and Unsicker K: GDNF prevents TGF-beta-induced damage of the plasma membrane in cerebellar granule neurons by suppressing activation of p38-MAPK via the phosphatidylinositol 3-kinase pathway. *Cell Tissue Res* 331: 373-383, 2008.
49. Kello M, Kulikova L, Vaskova J, Nagyova A and Mojzis J: Fruit peel polyphenolic extract-induced apoptosis in human breast cancer cells is associated with ROS production and modulation of p38MAPK/Erk1/2 and the akt signaling pathway. *Nutr Cancer* 69: 920-931, 2017.
50. Pan H, Yu M, Chen M, Wang X, Zhang H, Du S and Yu S: miR-126 suppresses neuronal apoptosis in rats after cardiopulmonary resuscitation via regulating p38MAPK. *Hum Exp Toxicol* 39: 563-574, 2020.
51. Matei N, Camara R and Zhang JH: Emerging mechanisms and novel applications of hydrogen gas therapy. *Med Gas Res* 8: 98-102, 2018.



This work is licensed under a Creative Commons Attribution-NonCommercial-NoDerivatives 4.0 International (CC BY-NC-ND 4.0) License.